THE ASTROPHYSICAL JOURNAL, 450:811–823, 1995 September 10

WIND-WIND INTERACTION IN THE CLOSE WOLF-RAYET BINARY CQ CEPHEI (WN6+O9 II–Ib)

S. V. MARCHENKO,[1,2] A. F. J. MOFFAT,[1] P. R. J. EENENS,[3] G. M. HILL,[1] AND A. GRANDCHAMPS[1,4]

Received 1994 December 28; accepted 1995 March 24

ABSTRACT

A large collection of blue and yellow CCD spectra of the short-period eclipsing binary CQ Cep allows us to improve the double-line (SB2) orbit of Kartasheva & Snezhko and reclassify the system as WN6+O9 II–Ib. With orbital inclination $i = 78°$–$65°$, the masses and radii are $M_O = 18$–$23\ M_\odot$, $M_{WR} = 15$–$19\ M_\odot$, $R_O \leq 10\ R_\odot$, $2\ R_\odot \leq R_{WR} \leq 10\ R_\odot$. For its spectral type, the O star mass and radius are smaller than values deduced from evolutionary models but agree with recent determinations of other O stars in binaries. The W-R star is shown to contain a small amount of hydrogen in its wind.

Because of the rapid orbit revolution compared to the wind velocities, the wind interaction zone is tightly wrapped around the system. We construct a phenomenological model which explains the numerous phase-dependent spectral variations.

Subject headings: binaries: eclipsing — stars: early-type — stars: fundamental parameters — stars: Wolf-Rayet

1. INTRODUCTION

CQ Cep = WR 155 = HD 214419 (WN7+abs, according to van der Hucht et al. 1988) is the massive W-R binary with the shortest known period. Its photometric, spectroscopic, and polarimetric properties have been summarized most recently by Stickland et al. (1984), Kartasheva & Svechnikov (1990), Drissen et al. (1986), and Underhill, Gilroy, & Hill (1990):

1. The light curve shows two deep, broad minima with clear ellipticity effects and is subject to frequent large-amplitude cycle-to-cycle variations ranging from ~0.05 to 0.1 mag.
2. The system has a very complicated history of changes in orbital period (Kartasheva & Svechnikov 1990); however, the period has not *significantly* changed over ~30 yr of photometric observations (Walker et al. 1983).
3. The radial velocity (RV) curves of practically all absorption lines move in phase with the W-R star emission lines; the shape of the He II λ4686 emission RV curve is peculiar (Leung, Moffat, & Seggewiss 1983; Stickland et al. 1984).
4. The line profiles are variable, exhibiting a pronounced stochastic component. However, the orbital phase-related structural changes seem to dominate over the random variations on the long term (Leung et al. 1983).
5. The photometrically and polarimetrically derived orbital inclination ranges from 65° to 78° (Lipunova & Cherepashchuk 1982; Piirola & Linnaluoto 1988) with some preference for 74° ± 4° (Drissen et al. 1986).
6. The companion can be classified as an O6–B0 star; the presence of a compact companion can be definitely ruled out.
7. Niemela (1980) found antiphase motion relative to the W-R star of the absorption components of He II λ4686 and He I λ3889, and Kartasheva & Snezhko (1985) revealed the presence of O star absorption lines across the entire CQ Cep spectrum in the optical region. The results of Niemela (1980) are contradicted by those of Leung et al. (1983) and Stickland et al. (1984), who were unable to confirm the presence of the He II λ4686, He I λ3889 O star absorptions. Underhill et al. (1990) question the detection of an O companion on the basis of the large published difference between the derived and expected Galactic systemic velocity of the O star in CQ Cep.

Since the publication of Underhill et al. (1990), no efforts have been made to clarify the nature of the companion. Here we report the identification of the companion's spectral features, derive the orbit of both components, and discuss some details of the wind-wind interaction.

2. OBSERVATIONS

All data considered in this investigation have been obtained in 1986–1994. RVs obtained from all but the Underhill et al. (1990) data are given in Table 1: column (1) is the heliocentric JD of mid-exposure; column (2) is the observatory; column (3) is the orbital phase in accordance with the comprehensive photometric study of Walker et al. (1983); column (4) is the measured heliocentric RV of the relatively strong, unperturbed emission line N IV λ4058; and the remaining columns are the RVs of the O star absorption lines of He I λ4471, Hδ, and Si IV λ4116, if measurable in a given spectrum. The first 17 spectra were obtained in 1988–1989 at the Mont Mégantic (MM) Observatory (Québec, Canada) at the Cassegrain focus of the 1.6 m telescope equipped with a Boller & Chivens spectrograph and an RCA 512 × 320 CCD, with resolution $\Delta\lambda = 3.3$ Å (2.4 pixels) in the range λλ3600–4200 and S/N ~ 100–150 per pixel in the continuum (Grandchamps & Moffat 1991). We have completed the Mont Mégantic collection by four spectra taken there in 1994 July (Thompson 1024 × 1024 CCD, $\Delta\lambda = 2.4$ Å (2.9 pixels) in the range λλ3720–4560 and S/N ~ 170–250). Seventeen more spectra were taken at the 2.1 m telescope + Cassegrain spectrograph + Thompson 1024 × 1024 CCD at the San Pedro Martir (SPM) Observatory (Baja California, México) during 1993 September–October, $\Delta\lambda = 1.9$ Å (2.3 pixels) in the range λλ3980–4830 or λλ4120–4970 and S/N ~ 120–180. The third source of data comes from Under-

[1] Département de Physique, Université de Montréal, C.P. 6128, Succursale Centre-Ville, Montréal, QC H3C 3J7, Canada, and Observatoire du Mont Mégantic; sergey,moffat,hill@astro.umontreal.ca.
[2] On leave from Main Astronomical Observatory of the Ukrainian Academy of Sciences, Goloseevo, 252127 Kiev, Ukraine.
[3] Instituto Nacional de Astrofísica, Optica y Electrónica, Apdos. Postales 216 y 51, Puebla 72000, Pue., México; eenens@tonali.inaoep.mx.
[4] Now at Planétarium de Montréal, 1000 Rue St. Jacques Ouest, Montréal, QC H3C 1G7, Canada.

TABLE 1

SUMMARY OF THE MONT MÉGANTIC AND SAN PEDRO MATIR OBSERVATIONS

			RV (km s^{-1})			
			W-R	O Star Absorptions		
HJD (−2,440,000) (1)	OBSERVATORY (2)	PHASE[a] (3)	N IV λ4057.80 (4)	Hδ 4101.73 (5)	Si IV λ4116.10 (6)	He I λ4471.48 (7)
7347.792.....	MM	0.068	−233	...	−15	...
7348.616.....	MM	0.570	95	...	−163	...
7490.623.....	MM	0.094	−271	...	65	...
7490.723.....	MM	0.155	−356	231	125	...
7730.604.....	MM	0.313	−340	222	150	...
7730.792.....	MM	0.428	−127	...	74	...
7731.608.....	MM	0.925	32	...	−235	...
7749.603.....	MM	0.889	98	...	−257	...
7749.840.....	MM	0.034	−173	...	−102	...
7753.688.....	MM	0.378	−239	...	22	...
7755.580.....	MM	0.531	14	...	...	...
7755.835.....	MM	0.686	198	...	−171	...
7757.584.....	MM	0.752	197	...	−191	...
7757.836.....	MM	0.906	69	...	−209	...
7762.589.....	MM	0.802	200	...	−186	...
7763.589.....	MM	0.411	−194	...	60	...
7765.812.....	MM	0.765	170	...	−203	...
9259.914.....	SPM	0.113	...	...	...	104
9260.930.....	SPM	0.732	...	...	...	−405
9261.884.....	SPM	0.313	...	...	...	136
9262.869.....	SPM	0.913	...	...	...	−150
9263.832.....	SPM	0.500	−17	...	102	−135
9263.862.....	SPM	0.518	11	...	...	−213
9263.925.....	SPM	0.557	60	...	...	−215
9264.731.....	SPM	0.048	−173	...	−125	180
9264.830.....	SPM	0.108	−294	166	−14	165
9264.903.....	SPM	0.153	−337	187	41	188
9265.696.....	SPM	0.636	201	...	−215	−254
9265.825.....	SPM	0.714	240	...	−233	−323
9265.896.....	SPM	0.758	202	...	−284	−345
9266.622.....	SPM	0.200	−338	238	61	134
9267.862.....	SPM	0.955	4	...	−212	...
9267.933.....	SPM	0.999	−82	...	−190	4
9554.666.....	MM	0.703	...	...	−199	...
9558.792.....	MM	0.217	−364	267	242	...
9561.685.....	MM	0.980	−23	...	−131	...
9561.766.....	MM	0.029	−143	...	−136	...

[a] According to ephemeris of Walker et al. 1983 for phase zero (primary light curve minimum): JD 2,415,000.410 + 1^d.6412436E.

hill et al.'s (1990) set of 22 spectra from DAO = Dominion Astrophysical Observatory ($\Delta\lambda$ = 0.9–1.4 Å [2–3 pixels] in the range $\lambda\lambda$5200–6000 and S/N ~ 120–695). For the sake of homogeneity and better compatibility with the MM and SPM data, all the DAO spectra were reextracted and reprocessed. The processing of the spectra and all subsequent measurements of the radial velocities (Fig. 1) and equivalent widths (Fig. 2) have been performed using standard IRAF procedures. In particular, the measurement of weak absorption features superposed on emission lines follows our procedure as outlined in a previous study of V444 Cygni (Cherepashchuk et al. 1995): we fit a Gaussian profile to the weak absorption allowing for a sloping local continuum.

3. NEW ORBITAL ELEMENTS AND QUANTIFICATION OF THE COMPONENTS

Most of the easily distinguished absorption features move in phase with the W-R star emissions. However, careful inspection of the whole data set reveals some interesting details. In Figure 3 two weak absorption dips superposed on the He II λ4100 emission profile seem to move in antiphase with the W-R emission features. If arising from the photosphere of the O star companion, these absorption components are likely due to Si IV λλ4089, 4116. Other absorption features, probably originating from the O star, can be seen. Some are very subtle, others less so. Absorption, due to He I λ4471, can be seen at practically all phases except $\phi \sim 0.7$–0.8, when it is blended with the broad absorption feature originating in the W-R wind (Fig. 4*a*). At $\phi \sim 0.1$–0.4, conditions of blending are less severe so that one can also identify absorption from Hδ (Fig. 3; note the two modes of display for extra clarity), He II λ5412 (Fig. 4*b*), and other transitions, the motion of which implies an origin from the O star companion. These enable us to find important new orbital constraints for CQ Cep. We combine our RV data for the clearest O star absorptions (He I λ4471, 15 measurements at practically all phases; 5875, three measurements at ϕ = 0.940, 0.947, 0.961; He II λ5412, three measurements at ϕ = 0.119, 0.177, and 0.214; and Hδ, six measurements at ϕ = 0.108–0.313) and the best W-R (pure) emission line of N IV λ4058, with the N IV λ4058 RV measurements of Bappu &

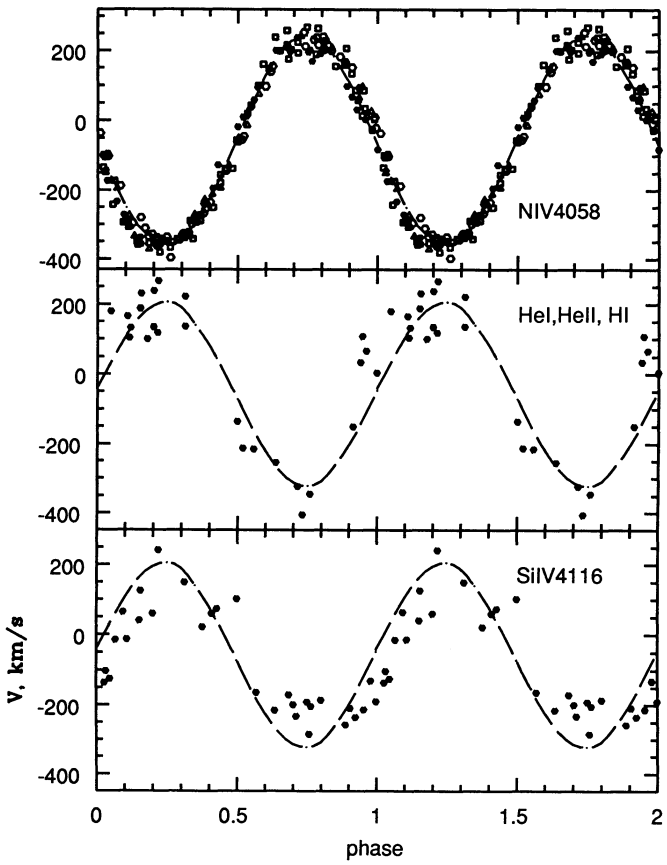

FIG. 1.—Radial velocity variations as a function of orbital phase based on the Walker et al. (1983) light curve ephemeris ($\phi = 0$ corresponds to primary minimum, when the O stars is in front). The orbital solution for N IV λ4058 emission and the H, He absorption lines is shown by a dashed line. Open squares, triangles, and circles, and filled circles, indicate the data of Bappu & Visvanadham (1977), Leung et al. (1983), and Stickland et al. (1984), and our data, respectively.

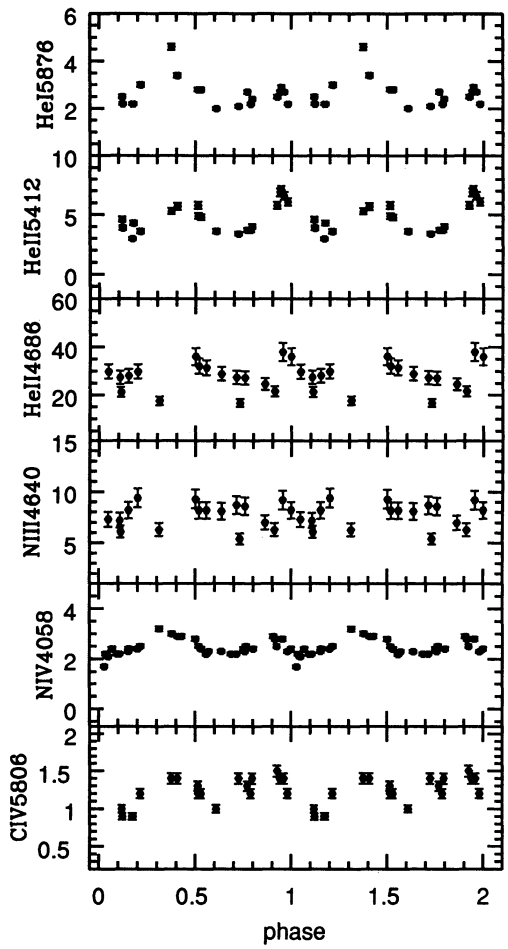

FIG. 2.—Equivalent width variations with phase of the most important emission lines. The 2 σ error bars of He I λ5876, He II λ5412, and N IV λ4058 are comparable with the size of the symbols.

Visvanadham (1977), Leung et al. (1983), and Stickland et al. (1984) (Fig. 1). The present RVs for N IV λ4058 have been derived by calculating the centroid wavelength of the whole profile.[5] RV measurements of the O star absorptions have been performed by deblending the line contours or fitting a Gaussian profile using the "splot" task in the IRAF package. The orbital elements have been calculated (Table 2) by applying the Bertiau & Grobben (1969) algorithm with fixed period $P_0 = 1^d.6412436$ and γ_0, K, T_0, ω, and e as free parameters for a total of 166 measurements of N IV λ4058 emission and 27 measurements of the O star absorptions (He I $\lambda\lambda$4471, 5875, He II λ5412, and Hδ), giving 3 times more weight to the emission line. Taken alone, the RVs of the O star give a different value of the eccentricity, $e = 0.142 \pm 0.042$ (vs. $e = 0.034 \pm 0.008$), although the values of $K_O = 273.3 \pm 12.9$ km s^{-1} (vs. $K_O = 263.5 \pm 10.6$ km s^{-1}) and $\gamma_O = -50.1 \pm 9.9$ km s^{-1} (vs. $\gamma_O = -57.6 \pm 18.0$ km s^{-1}) remain practically unaffected, compared to the combined solution. We did not use the RVs of Si IV λ4116 to derive the orbital elements: sine-wave fitting to the RV curves of Si IV λ4116 yields semiamplitude $K_O = 180$ km s^{-1}, much lower than $K_O = 264$ km s^{-1} from the above He, H lines. The value of K_O from Si IV λ4116 O star absorption is affected by blending (Si IV λ4089 is even worse) with the underlying Si IV W-R emission feature, both emission and absorption having comparable width and moving in antiphase. When we are dealing with the He I, II absorptions, the underlying emission is much broader, so that distinguishing of the absorption is an easier task.

Underhill et al. (1990) concluded that (based on its galactic location) CQ Cep should have a systemic velocity between -65 and -25 km s^{-1}. Previous claims of detection of O star absorption lines in CQ Cep were rejected by Underhill et al. (1990) based on the derived systemic velocities not falling within this range. We find a systemic velocity for CQ Cep derived on the O star absorption lines of -58 ± 18 km s^{-1}.

Can gas streams mimic the appearance of the redshifted absorptions at $\phi \sim 0.1$–0.4, instead of arising in the O star

[5] A search for any systematic differences of the velocities derived for the full profile compared to those derived from its upper part, (0.5–1.0) I_{max}, sometimes shows at certain phases small deviations slightly exceeding the 1 σ measurement accuracy, σ(RV) = 11 km s^{-1} for the MM data and σ(RV) = 16 km s^{-1} for SPM. The small value of eccentricity (Table 2) is probably the result of systematic deviations caused by phase-related profile variations. For consistency with previous authors, we ignore the source of these variations and derive the N IV RV orbit-based face value on the whole profile. Generally, we observe N IV λ4058 as a symmetric profile with variable I_{max} as the only obvious phase-dependent variation (Figs. 2 and 5). Forcing the eccentricity to zero leads to values of K_O and K_{WR} which differ by at most 3% from the eccentric ones.

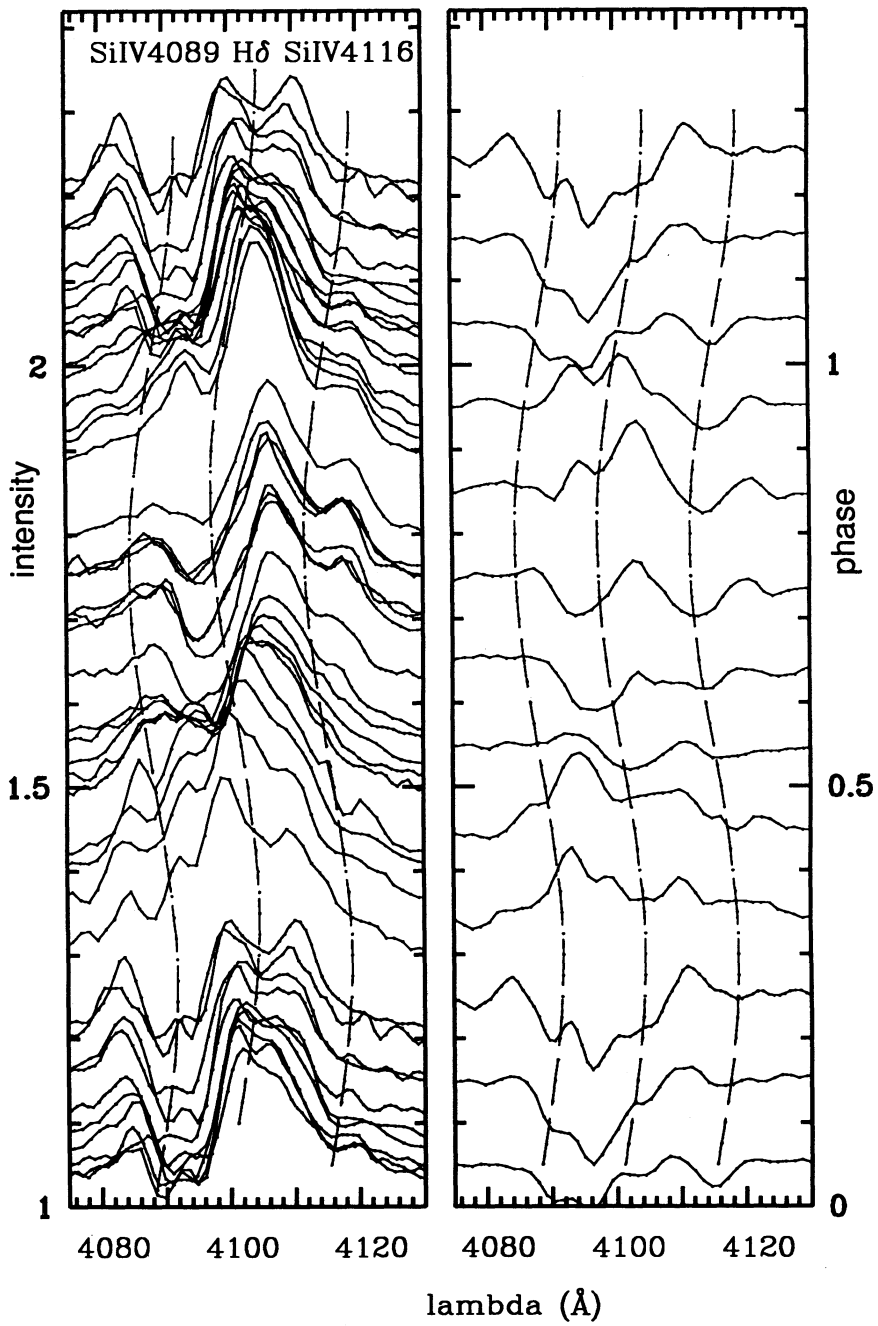

FIG. 3.—Montage of the spectra for the λλ4075–4135 region. *Left*: for the observed spectra. *Right*: after subtracting off the mean W-R spectrum (as in Fig. 6) and binning to 0.1 in phase. The orbits of the Hδ and Si IV λλ4089, 4116 O star absorptions are marked by dashed lines. Each spectrum is renormalized to allow for the variable continuum level (eclipses; see text).

TABLE 2

NEW ORBITAL ELEMENTS AND MASSES OF THE COMPONENTS FOR CQ CEPHEI[a]

Object	γ_0 (km s^{-1})	K (km s^{-1})	T_0 (−2,440,000)	ω	e	$a \sin i$ ($R_\odot$)	$M \sin^3 i$ ($M_\odot$)
W-R star.....	−58.5	303.2	7730.988	113°2	0.034	9.8	14.4
	±1.7	±2.4	±0.002	±13.3	±0.008	±0.1	±1.1
O star.....	−57.6	263.5	...	...	...	8.5	16.6
	±18.0	±10.6	...	...	...	±0.3	±1.3

NOTE.—γ_0 = systematic velocity, K = RV amplitude, T_0 = time of periastron passage, ω = angle between ascending node and periastron, e = eccentricity, and $a \sin i$ = semimajor orbital axis.

[a] Based on N IV λ4058 for the W-R component and He, H absorption lines for the O star.

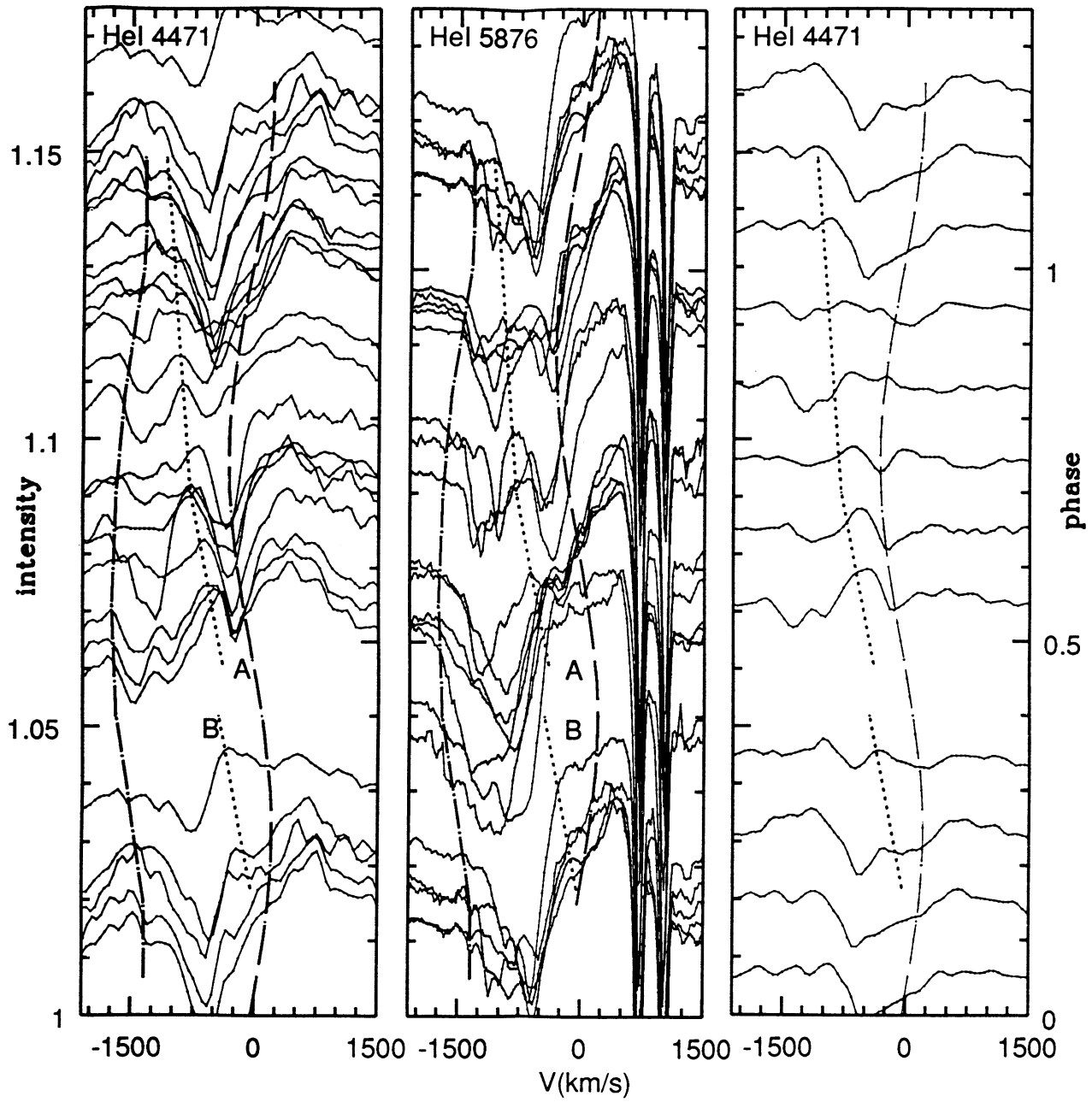

FIG. 4a

FIG. 4.—(*a*) Variations of He I λ4471 (*left panel*) and He I λ5876 (*central panel*) with phase. The right panel refers to He I λ4471 after subtracting off the mean W-R spectrum (as in Fig. 6) and binning to 0.1 in phase. The shift of the extra emission component arising in the wind-wind interaction zone is shown by a dotted line. The change of the W-R wind terminal velocity is shown by a dash-dotted line. A dashed line denotes the O star orbit. Each spectrum is renormalized to allow for the variable continuum level (eclipses). The intensity scales are different (increased by 7.7 times for He I λ5876 compared to He I λ4471). (*b*) Variations of He II λ4200 (*left panel*) and He II λ5412 (*right panel*) with phase. The shift of the extra emission component arising in the wind-wind interaction zone is shown by a dotted line. A dashed line denotes the O star orbit. Each spectrum is renormalized to allow for the variable continuum level (eclipses). (*c*) Variations of N V λ4604 (*left panel*) and He II λ4686 (*right panel*) with phase. A dashed line denotes the O star obit. Each spectrum is renormalized to allow for the variable continuum level (eclipses).

photosphere? One could assume a semidetached system, with the O star component filling its Roche lobe and the gas streaming toward the W-R star through the inner Lagrangian point. Redshifted absorption would be observed when the gas stream is projected on the bright W-R disk, i.e., around $0.1 \leq \phi \leq 0.2$. However, the same gas should appear as emission, starting at $\phi \sim 0.2$. This is not the case for the strong Hδ (Fig. 3) and He II λ5412 (Fig. 4*b*) absorption features; hence, we consider this interpretation for these absorptions less likely.

For the possible range of $i = 78°$–$65°$, the masses of the components and the orbital separation are: $M_O = 17.7$–22.3 $M_\odot$, $M_{WR} = 15.4$–19.4 $M_\odot$, $a = 19.7$–24.7 $R_\odot$. Note that for $i \geq 65°$, the separation between the components must be large enough to allow the absorption component of N V λ4604 to be

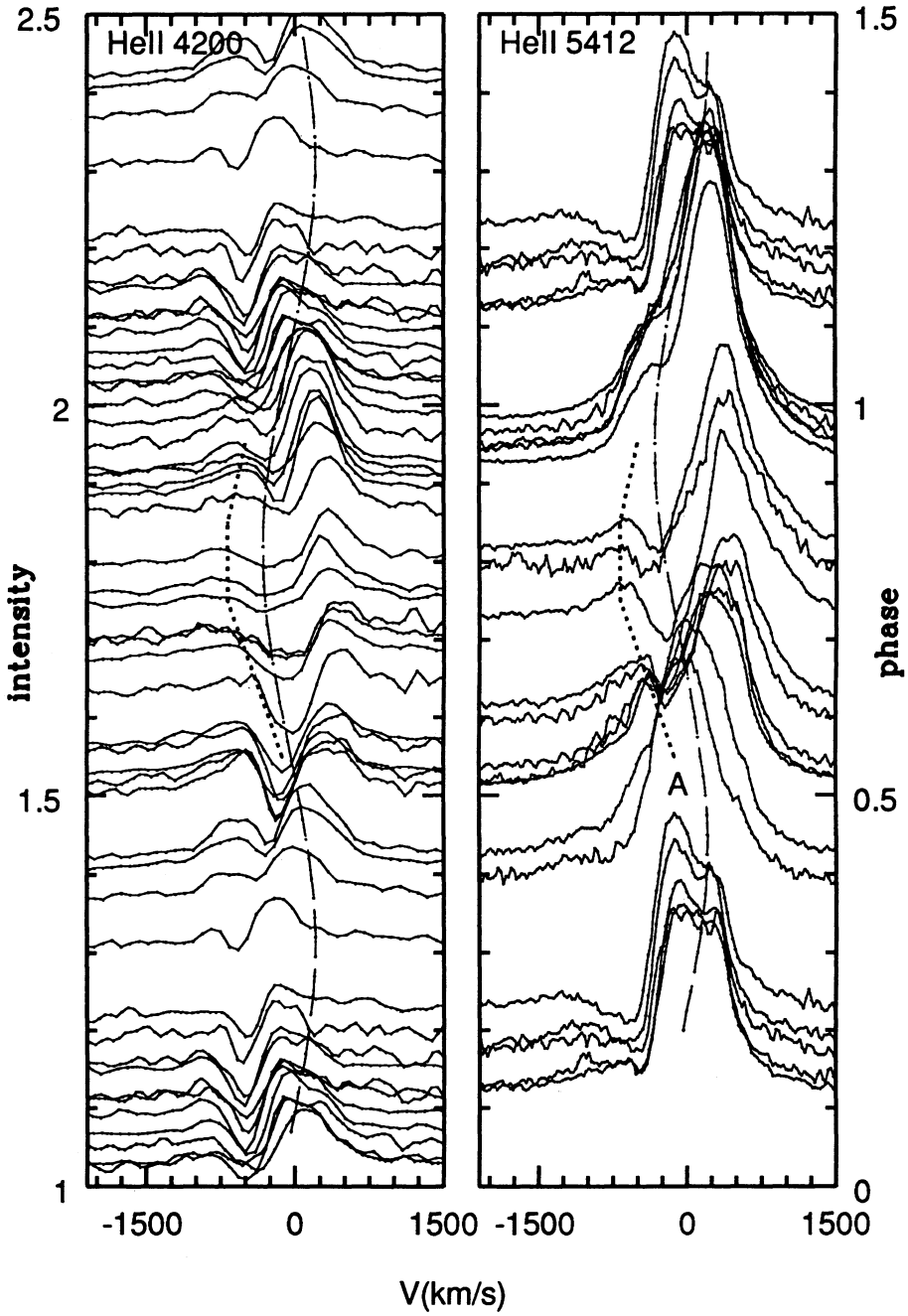

FIG. 4*b*

formed at $\phi \sim 0.0$ (O star in front). This component remains practically unaffected (see second panel of Fig. 5) during the geometric eclipse of the bright part of the W-R wind, i.e., the region where τ(electron scattering) ≥ 1. This means that the O star radius $R_O \leq 10\ R_\odot$ (i.e., approximately the Roche lobe radius of the O star), and the W-R radius must satisfy $2\ R_\odot \leq R_{WR}(\tau_{es} \geq 1) \leq 10\ R_\odot$. Thus, the system must be detached or semidetached, to maintain the unperturbed N v absorption feature, or the orbital inclination must be much less than 65°, in obvious contradiction especially with the estimate of $i = 78°$ from polarimetry. However, the polarimetric values are based on the assumption of spherically symmetric winds and should be taken with some caution. The R_O value appears to be too low for an average standard O9 II-Ib star (see below), which usually lies in the range of 14–30 $R_\odot$ (Howarth & Prinja 1989; Herrero et al. 1992). However, sophisticated Doppler tomography of several O8–9 II-I type binaries leads to much lower $R_O \sim 10$–13 $R_\odot$ (Penny, Bagnuolo, & Gies 1993), in better agreement with our estimate for the O star in CQ Cep. Further support for a small R_O value comes from measurements of FWHM for the Si IV λ4116 and He I λ4471 lines: 6.4 Å and 6.2 Å ($\pm$1.2 Å), respectively. Converting this FWHM to the rota-

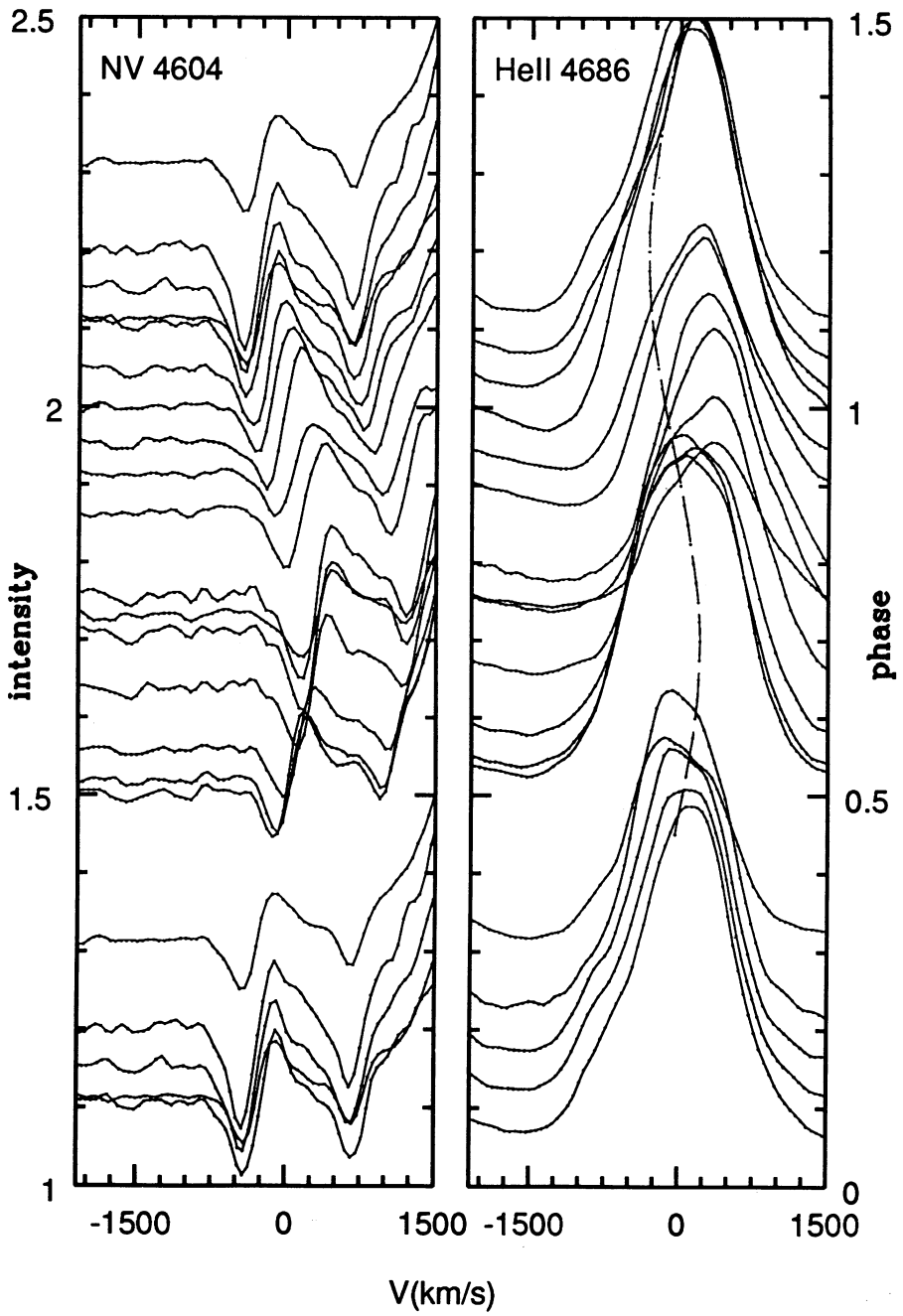

FIG. 4c

tional velocity of the O star leads to an estimate of the O star radius $R_O = 6$–$9\ R_\odot$, assuming orbit-rotation alignment and synchronization.

The masses of O9–9.7 supergiants, $M_O = 38$–$33\ M_\odot$, derived from sequences of evolutionary models (Howarth & Prinja 1989), are systematically higher (up to 2 times) than those observed. This must be a result of the well-known O star mass discrepancy (Herrero 1993). Our value of $M_O = 18$–$22\ M_\odot$ for CQ Cep falls well within the range of empirical masses obtained without any evolutionary assumptions, M(O7.5–9.7 II–I) = 12–22 $M_\odot$ (Penny et al. 1993; Herrero et al. 1992). Our value of $q = M_{WR}/M_O = 0.87 \pm 0.04$ is in good agreement with $q = 0.83 \pm 0.07$ from Kartasheva & Snezhko (1985). However, our $M \sin^3 i$ values are higher (14.4 and 16.6 vs. 11.7 and 14.1 $M_\odot$, respectively) than those of Kartasheva & Snezhko (1985), as a result of different approaches of deblending the W-R + O absorption lines.

In an attempt to classify the O-type companion, we cannot apply the usual luminosity and spectral criteria (Conti & Alschuler 1971; Bagnuolo et al. 1994) for any individual spectrum, due to the faintness of the O star features. (A method to enhance their visibility will be explored below.) Comparison of the relative absorption strengths of Hδ, Si IV $\lambda\lambda$4089, 4116, and He I λ4121 in the digital atlas of Walborn & Fitzpatrick (1990) leads to the following conclusion: if the O star has luminosity class III–V, the spectral class must be O8–8.5, as a result of

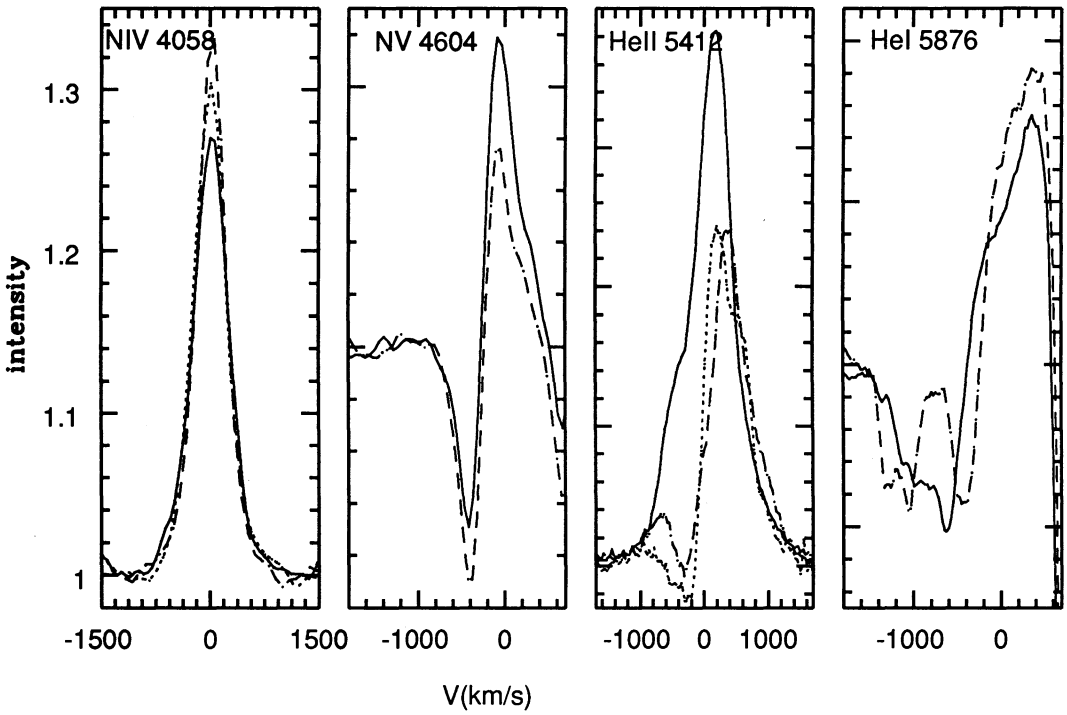

FIG. 5.—Orbit-related profile variations of (from left to right): N IV λ4058 (*first panel*)—the full line denotes the mean of $n = 3$ spectra at $\phi = 0.990$, the dashed line corresponds to the mean ($n = 3$) at $\phi = 0.758$, and the dotted line marks the mean ($n = 3$) at $\phi = 0.516$; N IV λ4604 (*second panel*)—the full line denotes the mean ($n = 3$) at $\phi = 0.001$, the dashed line corresponds to the mean ($n = 4$) at $\phi = 0.144$; He II λ5412 (*third panel*)—the full line denotes the mean ($n = 4$) at $\phi = 0.954$, the dashed line corresponds to the mean ($n = 3$) at $\phi = 0.764$, and the dotted line marks an individual profile at $\phi = 0.214$; He I λ5876 (*last panel*)—the full line denotes the mean ($n = 4$) at $\phi = 0.148$, the dashed line corresponds to the mean ($n = 3$) at $\phi = 0.764$. Each spectrum is renormalized to allow for the variable continuum level (eclipses) and shifted to zero velocity by the known RV of the W-R component before averaging. The intensity scales are different (reduced by 0.6 times for N V λ4604, increased by 1.2 times for He I λ5412, and unchanged for He I λ5876 relative to N IV λ4058).

rapid disappearance of Si IV in hotter stars and rapid growth of He I λ4121 in O9–B0 subclasses. If the luminosity class is II–I, then the most probable spectral class is O8.5–O9.5: the EW of the Si IV λ4116 absorption is (very roughly!) 2–4 times less than the Hδ O star absorption component, and He I λ4121 is practically absent, being partially blended by the broad Si IV λ4116 absorption. Note that the O star Si IV absorption lines overlap with the Si IV emission components arising in the W-R star. The latter are not well developed and are completely dominated by the O star absorptions around phases 0.9–1.2. The best phases to see the Si IV λ4116 W-R star emission are at $\phi \sim 0.6$–0.8. Indeed, one can notice the redshifted weak emission at $\lambda \sim 4118$–4120 Å (Fig. 3), that is gradually replaced by the O star absorption toward $\phi = 0.0$. The overall appearance of the CQ Cep spectrum closely resembles that of the SB1 binary WR 22, a WN7 star with a deduced (i.e., not directly seen in the spectrum) O9 V companion (Crowther et al. 1995a, b). Comparison of the *IUE* UV spectra of CQ Cep and WR 22 (St-Louis 1990) allows one to restrict the classification of the O component in CQ Cep. The emission component of Si IV λ1402, arising in both the O star and the W-R star, is much weaker in CQ Cep than in WR 22, but the remaining prominent emission features have compatible strengths. The luminosity ratio of the CQ Cep components is close to unity. If the O star in CQ Cep is of luminosity class Ia, this should lead to strengthening of the Si IV emission (see spectral atlas of Walborn, Nichols-Bohlin, & Panek 1985), contrary to what is observed. Hence, the luminosity class can be restricted to "below Ia," with some reference for II, considering the additional argument about the detached or semidetached character of the system and the observed line ratios discussed above.

The relatively reliable EWs of Si IV λ4116 and He I λ4471 have been used to derive the luminosity ratio, L_{WR}/L_O. After allowing for the variable continuum level[6] and correcting for the intensity of the underlying emission (as in Beals 1944), the mean observed value of the EW is W_{bin}(Si IV λ4116 + He I λ4121) = 0.32 ± 0.13 Å (24 spectra). (Note that the Si IV line has large width, FWHM = 6.4 Å, and is blended with He I λ4121, so that the EW includes both lines). The mean "standard" values of EW for Si IV λ4116 + He I λ4121 in single O8–O8.5 V–III and O8.5–O9.5 II–I stars are $W_{std} = 0.30$ and 0.51 Å, respectively (Conti & Alschuler 1971). The classification of the companion as O8–O8.5 V–III must be rejected because W_{bin} would significantly exceed W_{std} in that case, accounting for the dilution of the O star features by the W-R companion (see below). Using Beals's (1944) method, we obtain the luminosity ratio: $L_{WR}/L_O = W_{std}/W_{bin} - 1 = 0.6 \pm 0.2$.

Measurement of EW(He I λ4471) is less reliable, due to the more complicated way of determining the local "continuum" level and deblending from the blueshifted W-R star absorption. Therefore, we decided to measure the EW of He I λ4471 using the mean spectrum (combination of 17 spectra) obtained in the

[6] To correct the spectra for the CQ Cep light curve to true relative line flux, we have used the averaged *V*-filter light curve (Antokhina & Cherepashchuk 1988). The correction has been performed applying the formula: $I_\lambda^{corr}(\phi) = C(\phi)(I_\lambda^{uncorr} - 1) + 1$, where $I_\lambda(\phi)$ denotes the intensity in the corrected or uncorrected rectified spectrum and $C(\phi)$ is the normalized [maximum value is $C(\phi) = 1$] light curve.

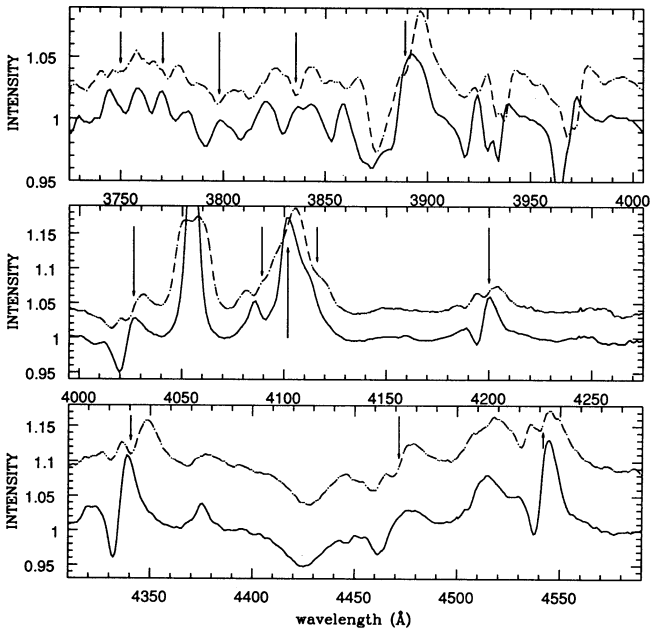

FIG. 6.—Co-added normalized spectra, shifted by the mean orbit to the frame of the W-R star (*solid line*) and the O star (broken line). For clarity, the O spectra are offset in intensity from those of the W-R star. The O-star absorption lines discussed in text are marked by arrows.

following manner. After renormalization for variable continuum level (eclipses), each spectrum was shifted by the known RV orbit of the O star to the O star frame of reference, and co-added (see Fig. 6). The O star line can then be easily distinguished because the underlying W-R profile is smeared out by large, artificial shifts, RV(O) + RV(WR). We have derived W_{bin}(He I λ4471) = 0.30 ± 0.05 Å, which with W_{std}(He I λ4471) = 0.83 Å for O8.5–9.7 II–I stars (Conti & Alschuler 1971; Bisiacchi, Lopez, & Firmani 1982; Mathys 1988, 1989). gives $L_{WR}/L_O = 1.8 \pm 0.3$.

For better consistency we remeasured the EW(Si IV λ4116 + He I λ4121) value in the mean spectrum (total of 32 spectra) shifted to the RV frame of the O star, as was done for the He I λ4471 line. We obtain W_{bin}(Si IV λ4116 + He I λ4121) = 0.25 ± 0.05 Å, and thus $L_{WR}/L_O = 1.0 \pm 0.3$. Combining both estimates obtained from the mean shifted spectrum with weights proportional to the number of observations, (Si IV λ4116 + He I λ4121):He I λ4471 = 2:1, we obtain $L_{WR}/L_O = 1.3 \pm 0.2$. The error was calculated using the method of error propagation.

Looking at the artificially "enhanced" spectrum of the O star (by RV shifting to the O star frame and co-adding the spectra), we find independent support for our spectral classification. The O star absorption at He II λ4686 is very weak (Fig. 4*c*) and invisible in the mean "enhanced" spectrum due to unfavorable dilution by strong emission; and EW(He II λ4686 + He I λ4388) ~ 0.10 Å (accounting for the luminosity ratio ~1), which is too small to be classified as a star of luminosity class III, and far from the main-sequence value (Mathys 1988). The ratio of $\log_{10}[W_\lambda(4471)/W_\lambda(4542)]$, the best criterion of O star spectral classes (Mathys 1988), is 0.36 ± 0.12, nicely within the 0.30–0.45 range for an O9 star.

Shifting all the available spectra to the RV frame of the W-R star (Fig. 6) smears out weak and reduces strong O star absorptions and thus yields a cleaner net W-R spectrum, neglecting any phase-dependent variability of the profiles. Unlike the unshifted O star absorption lines, all W-R star absorptions are blueshifted by $\sim -200 \pm 50$ km s^{-1}. This is common in WN6–7 stars and means that all W-R H, He I, II absorptions are formed in practically the same region of the expanding W-R atmosphere.

The W-R component of CQ Cep has been classified as WN7 by Smith (1968) and WN6 by Walborn (1974). To investigate the possible source for this discrepancy, we plotted the new classification criterion values (Smith, Shara, & Moffat 1995) versus orbital phase (Fig. 7). The ratio of peak line intensity, I_{max} of He II λ5412 to I_{max} of He I λ5876, is used as the principal criterion to define the WN subclass. Obviously (upper panel of Fig. 7), this ratio for CQ Cep is grouped around 1.5, close to the boundary value between WN6 and WN7 subclasses. The W-R component can be classified as WN6 around $\phi \sim 0.0$ (O star in front); this emphasizes the significance of the wind-wind interaction effects (see below). One can explore two additional criteria, I_{max}(N V λ4604)/I_{max}(N III λ4640) and I_{max}(N IV λ4058)/I_{max}(N III λ4640), to distinguish between WN7 and WN6. The tendency of an earlier W-R spectrum around phase $\phi \sim 0.0$ is also seen in the $I_{max}(4604)/I_{max}(4640)$ ratio, as well as

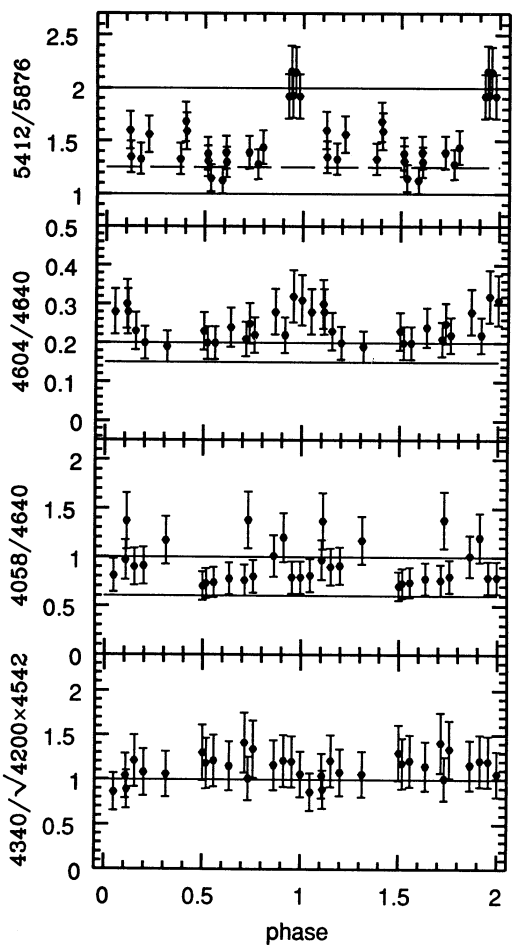

FIG. 7.—Phase dependence of intensity ratios for different lines used as classification criteria is shown together with 2 σ error bars. The WN6 (lower) and WN7 (upper) mean values are denoted by full horizontal lines. The dashed line for the "5412/5876" section denotes the boundary between WN6 and WN7. The line at 1.0 in the "hydrogen" section corresponds to the level of no detectable hydrogen.

in $I_{max}(5412)/I_{max}(5876)$. The overall estimated W-R subclass for CQ Cep lies between WN6 and WN7, with some preference for WN6, which we adopt.

Assuming both components of CQ Cep to be normal for their spectral types leads to $M_v(\mathrm{WN6–7}) = -5.95$ (van der Hucht et al. 1988) and $M_v(\mathrm{O9\ II–Ib}) = -6.05$ (Schmidt-Kaler 1982). With cosmic scatter $\sigma(M_v) \sim 0.5$ mag one finds $L_{WR}/L_O \simeq 0.9^{+0.8}_{-0.4}$, compatible with the above estimates.

Finally, we investigate the question of hydrogen abundance in the W-R wind. Following Smith et al. (1995), we calculate the emission ratio $R(\mathrm{H/He}) \equiv I_{max}(4340)/[I_{max}(4200) \times I_{max}(4542)]^{1/2}$ as a function of phase in Figure 7. (For H/He = 0, this ratio will be 1.0.) For CQ Cep, the ratio R(H/He) has a mean value 1.1 ± 0.1, implying that the W-R wind may have a small trace of hydrogen. We verify this on the shifted mean W-R spectrum in Figure 6, which yields $R = 1.2$. In the case of the W-R absorptions, we fit Gaussian profiles with sloping continuum and calculate their depths. These depths are plotted in Figure 8, from which we see that the He II + H I lines are ~15%–20% deeper than the *pure* Pickering lines of He II. This value is compatible with that from emission lines.

4. EVIDENCE OF WIND-WIND INTERACTION IN CQ CEPHEI

Analysing the *IUE* spectra of CQ Cep, Shore & Corcoran (1992) came to the conclusion that the O star wind is "frustrated" by the presence of a powerful W-R wind, and the system undergoes a "mild" wind-wind interaction (WWI) rather than an active wind-wind collision (WWC). Further evidence of WWI was presented by Stickland et al. (1984): their Figure 21 shows an enhanced outflow at $\phi \sim 0.2$ and 0.8, and a hot zone located near the O star and between the components. Many more details of WWI in CQ Cep can be revealed by synthesizing all available information concerning profile variations for UV and optical lines of different ionization potential.

The first piece of evidence for strong WWI comes from excess emission (seen only at negative RVs, due to severe blending at positive RVs) in He I, II lines, as found in Figures 4*a*–4*b*. To clarify its emission nature, we have plotted together the mean profiles of He I, II around $\phi \sim 0.75$ (when the excess emission appears strongest) and $\phi = 0.1$–0.2 (when weaker)—see Figure 5, third and fourth panels. Note that such excess emission in He I, II lines is found to occur in other well-studied

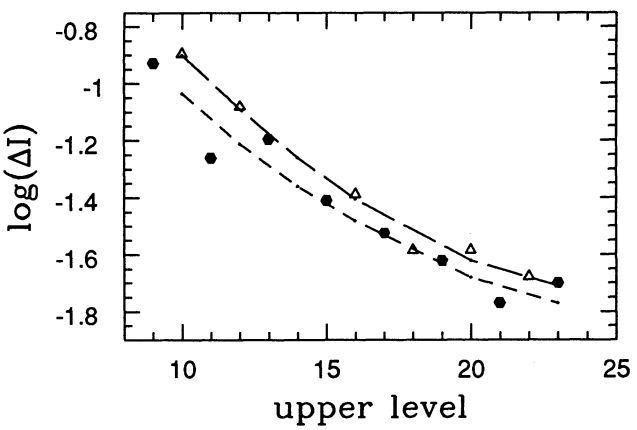

FIG. 8.—Dependence of the strength of the pure He II Pickering lines (*filled dots*) and He II Pickering lines diluted by H I Balmer lines (*open triangles*) on the upper transition level for He II. Curves indicate rough trends.

W-R + O systems with proven wind collisions: CX Cep (WN5 + O5 V, $P = 2.1$ days; Lewis et al. 1993) and V444 Cyg (WN5 + O6 III–V, $P = 4.2$ days; Marchenko, Moffat, & Koenigsberger 1994).

In Figure 9 we define two branches (A and B) of the shock zone. In He I, branch A appears to be stronger and reaches maximum negative RV (~ -1000 km s$^{-1} \ll v_\infty$) near $\phi \simeq 0.0$; branch B is weaker, and we cannot follow it after $\phi \sim 0.3$ due to its "projection" on the steepest part of the emission profile. In He II, only branch A is seen, with maximum negative RV at $\phi \simeq 0.75$ (Fig. 4*b*).

Branch A is stronger than branch B for the following reason. In close binary systems with strong tidal effects and one of the components (in this case, the O star) nearly reaching its Roche lobe, we expect the wind of the O star to be enhanced (but not to the point of being a true Roche lobe flow through L_1) in the direction toward the W-R star. Due to the Coriolis force, this enhanced wind must be deflected in the direction of the O star's orbital motion. This produces an asymmetry, with a more energetic wind interaction between the stars in the direction toward branch A than branch B (see Fig. 9). At greater distances from the stars, both branches are curved by the rapid orbital motion compared to the wind expansion velocities (see numerical calculations of Walder 1994).

Another fact can be added to support the idea of the bending of the WWI zone around the W-R star. Inspecting the profiles of He II λ5412 (Fig. 4*b*) around $\phi = 0.4$–0.5, one notices a lack of P Cygni absorption, contrary to what one would expect for an unperturbed W-R wind. This is likely caused by the cavity created by the O star in the W-R wind and bent outward beyond the W-R star (Fig. 9). If this cavity is situated right in the zone of He II λ5412 formation at $\phi \sim 0.4$, it will cause a reduction of the P Cygni absorption strength.

The remarkable random variations of the He I P Cygni absorptions (Fig. 4*a*) can be explained by thin shell and radiative instabilities arising due to fast cooling of the shocked gas (Stevens, Blondin, & Pollock 1992). The emission component of He II is expected to be less affected by radiative instabilities (see Fig. 4*b*), since it is formed closer to the stagnation point, in a zone with small volume and small outflow velocity.

The dependence of equivalent width (EW) on orbital phase was shown in Figure 2. All EWs are renormalized to allow for the continuum level changes, in accordance with the mean V-band light curve (Antokhina & Cherepashchuk 1988). The figure confirms previous findings (e.g., Stickland et al. 1984): there are two maxima in EW, with phase lag $\Delta\phi \leq -0.1$ relative to the light curve minima at phases 0.0 and 0.5. Due to the presence of a luminous O companion and WWI zone, one can expect to see some brightening of the part of the W-R wind facing the O star (Fig. 9). In addition, some emission comes directly from the WWI zone. The fractions of WWI emission and brightened wind emission are different for lines with different excitation and elements of different ionization level. Because of the lack of any pronounced phase variations in N IV, V (contrary to He I, II: see Fig. 5), we can assume that the emission from WWI is negligible for N IV, V and practically all EW variations are caused by the brightened portion of the wind, which follows the W-R orbital motion. For the He I, II lines, a significant amount of excess emission arises in the WWI zone, which can explain the peculiar shape of the He II λ4686 RV curve (e.g., Leung et al. 1983). For both types of extra emission, maximum flux is expected when the WWI and brightened zone have a maximal projected surface, i.e., around

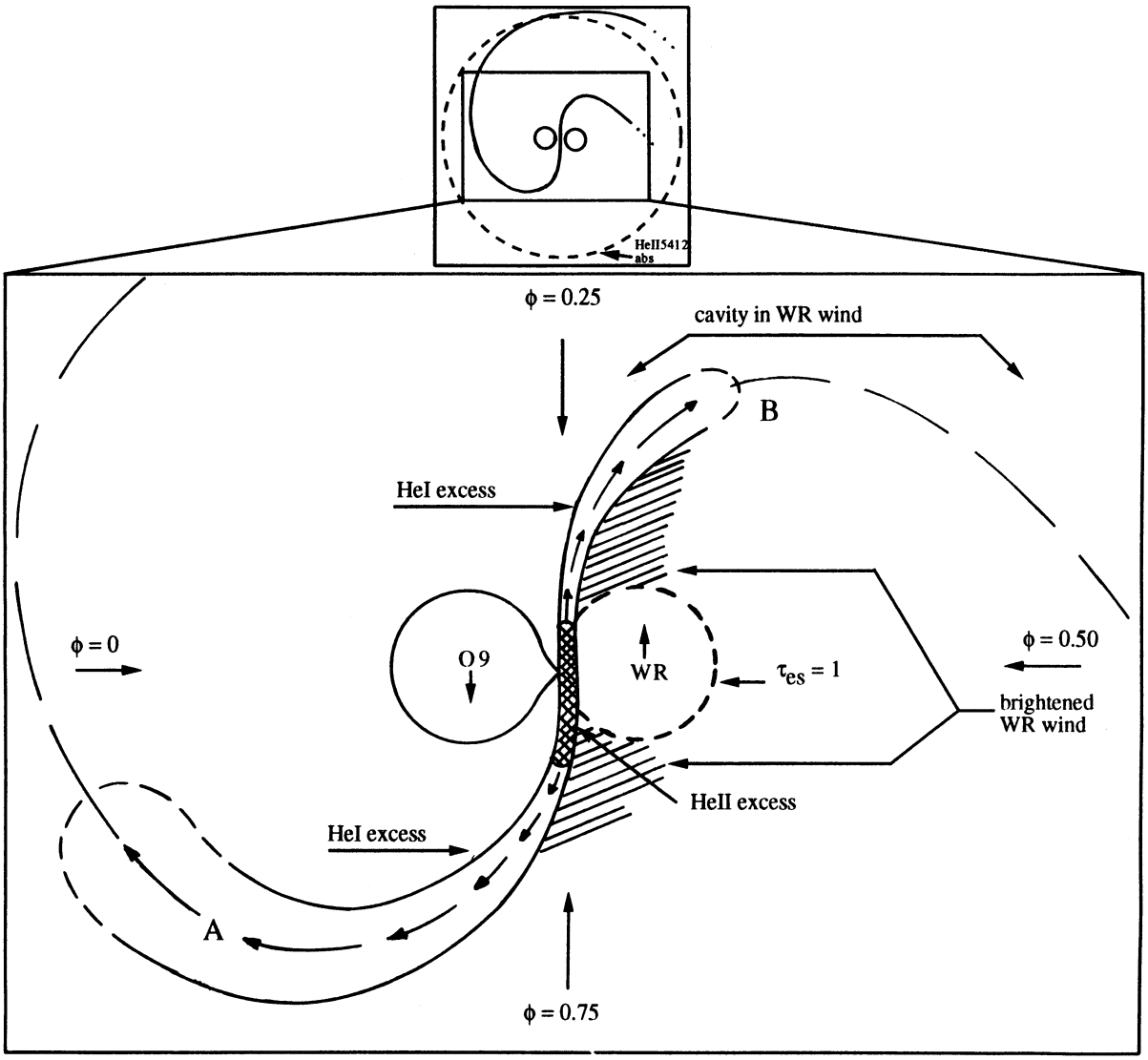

FIG. 9.—A cartoon showing our interpretation of the wind-wind interaction in CQ Cep

$\phi = 0.0$. The asymmetry in the brightness of the WWI zone (Fig. 9) accounts for the negative phase lag ($\Delta\phi \leq -0.1$) during its eclipse around $\phi \sim 0$. However, we might ask why the EW maximum is lacking for He I λ5876 at $\phi \sim 0.9$, the only "peculiarity" in Figure 2. The probable answer is that a large proportion of additional He I flux arises in the WWI zone mainly from branch A and is shifted to large negative velocity ($\leq v_\infty$) as $\phi \rightarrow 0$ (Figs. 4*a* and 9). Because we have been measuring only the *emission* part of the He I profile, this extra blue-shifted emission has been excluded automatically at phases around 0.0. The negative phase lag around $\phi \sim 0.5$ has a different origin. In the case of close massive binaries, recent numerical simulations (Walder 1994) show that the unperturbed flow is restored after approximately half an orbit. Thus, starting from $\phi \sim 0.4$ the optical depth of the W-R wind grows gradually, reducing the strength of additional emission coming from the WWI zone and the brightened part of the W-R wind.

Another recognizable effect is the variation of the W-R wind terminal velocity with phase (Fig. 4*a*): in He I lines, v_∞ at $\phi = 0.5$ (W-R star in front) exceeds v_∞ at $\phi = 0.0$ by as much as 350 km s^{-1}. This reduction cannot be caused by the cavity in the W-R wind behind the O star because, due to wrapping of the WWI zone, this cavity will disappear at large distance from the W-R + O system, where the bulk of the He I λ5876 absorption is formed. The light pressure from the O star also plays an insignificant role: the RV difference between the profiles of N V λ4604 taken at $\phi = 0.0$ and $\phi = 0.14$ does not exceed 100 km s^{-1} (Fig. 5). The main factor which can lead to the reduction of v_∞ behind the O star is the shadowing of the W-R star by the cooler O9 II–Ib companion and, as a consequence, a less extended He I formation zone. On the other hand, the P Cygni absorptions of N IV λ1718 and C IV λ1550 are formed (relative to He I λ5876) closer to the W-R + O system. Their strengths (Fig. 18 of Stickland et al. 1984) are significantly reduced around $\phi \sim 0.0$. This phenomenon lasts about half a period, which leads to a great extent of the cavity behind the O star. The C IV λ1550 absorption also exhibits a second minimum (lacking N IV λ1718) around $\phi = 0.5$, when the W-R star is in front, with its wind dominating. To explain the difference between C IV λ1550 and N IV λ1718, we have to take into

account that the P Cyg absorption of C IV λ1550 is formed in both winds, while the N IV λ1718 P Cygni absorption is formed mainly in the W-R wind. This is why one observes two minima in C IV, caused by a reduction (compared to the phases $\phi \sim 0.25$ or 0.75) of absorbing material in the W-R wind at $\phi \sim 0.0$ and a reduction of absorbing material in the O star wind at $\phi \sim 0.5$.

All considered facts point toward a WWI zone having the shape of a plane between the stars and gradually bending outward due to orbital motion. Can the O star wind resist at all against a presumably much stronger W-R wind? As noted above, the answer is "yes," but only in a limited direction due to tidal Roche lobe–like flow and Coriolis forces. Outside this direction, the O star outflow is expected to be normal for an O star, but relatively weak compared to a W-R wind. The second argument in favor of the O star wind's ability to push back the W-R wind (at least) along the line joining the two stars is that the W-R component may in fact possess a relatively weak wind for its subclass. Indeed, comparison of EW for He I, II and N III, IV emissions in CQ Cep with the same emissions in the "single" WN6 stars WR 134, 136 (Barral et al. 1987) shows that the lines of CQ Cep are generally 3–10 times weaker, even allowing for 50% dilution due to the luminous companion. However, CQ Cep's lines are comparable with the EW of WN7 + abs stars (Crowther et al. 1995b). If the WN6 subclass applies to the W-R component of CQ Cep, then its W-R wind must be considered as weak.

Finally, we note that the *ROSAT* detection of CQ Cep yields $L_X(0.2\text{–}2.4\ \mathrm{keV}) = (0.05 \pm 0.98) \times 10^{32}$ ergs s^{-1}, which is very low compared to other W-R + O binaries (Pollock, Haberl, & Corcoran 1994). This is likely a consequence of (1) low wind speeds, (2) small extension of the expected X-ray–emitting WWI zone, and (3) rapid wrapping of the low-density shock cone around the system, so that keV X-rays are strongly attenuated in all directions.

5. CONCLUSIONS

Despite the complexity of the spectral variations in the close eclipsing binary CQ Cep, it is possible to account for them in the framework of wind-wind interaction in a rapidly revolving system. It is the proximity of the two stars and the near-supergiant nature of the O companion that makes CQ Cep appear unusual compared to the "normal" case when the strong W-R wind dominates the O star wind, as in V444 Cyg and CX Cep.

The main results of this investigation are the following:

1. Careful inspection of the absorption features in CQ Cep leads to a determination of the RV orbit for the O star companion. Combining this with the W-R star orbit leads to the following masses of the components: $M_O = 18\text{–}23\ M_\odot$ and $M_{WR} = 15\text{–}19\ M_\odot$ for orbital inclination $i = 78°\text{–}65°$. The geometry of the system and the phase variations of the N V λ4604 line restrict the radii of the stars to $R_O \leq 10\ R_\odot$, $2\ R_\odot \leq R_{WR} \leq 10\ R_\odot$.

2. The "enhancement" of the O companion spectrum by a "shift-and-add" procedure leads to its classification as O9 II–Ib. The spectral class of the W-R star is between WN6 and WN7, being closer to WN6.

3. The W-R wind contains some hydrogen because the pure Pickering He II lines (emission or absorption) are ~10%–20% less intense than the adjacent Pickering lines blended with the Balmer lines. In addition to the usual P Cygni profiles, some absorption lines of the W-R component are blueshifted (~ -200 km s^{-1}). Thus, strictly speaking, CQ Cep should be classified as WN6(h) + a + O9 II–Ib in the new three-dimensional system of Smith et al. (1995).

4. The wind-wind interaction zone is asymmetrical and is wrapped around both components, as a result of rapid orbital revolution. In the direction of the W-R star, the O star wind is able to resist the powerful W-R wind by virtue of tidal enhancement.

S. V. M. is grateful to CONACyT of México and the IAU for financial support. S. V. M., A. F. J. M., and G. M. H. acknowledge monetary aid from NSERC of Canada and FCAR (Québec). We thank Dave Stickland, the referee, for useful suggestions for improving the presentation. We thank Anne Underhill for allowing us to use the DAO spectra analyzed in this paper.

REFERENCES

Antokhina, E. A., & Cherepashchuk, A. M. 1988, Soviet Astron. 32, 531
Bagnuolo, W. G., Gies, D. R., Hahula, M. E., Wiemker, R., & Wiggs, M. S. 1994, ApJ, 423, 446
Bappu, M. K. V., & Visvanadham, P. 1977, Kodaikanal Obs. Bull. Ser. A, 2, 89
Barral, J. F., Bisiacchi, G. F., Firmani, C., Koenigsberger, G., & Wampler, J. 1987, Rev. Mexicana Astron. Af., 14, 284
Beals, C. S. 1944, MNRAS, 104, 205
Bertiau, F. C., S.J., & Grobben, J. 1969, Ric. Astron. Spec. Vaticana, 8, No. 1–2, 1
Bisiacchi, G. F., Lopez, J. A., & Firmani, C. 1982, A&A, 107, 252
Cherepashchuk, A. M., Koenigsberger, G., Marchenko, S. V., & Moffat, A. F. J. 1995, A&A, 293, 142
Conti, P. S., & Alschuler, W. R. 1971, ApJ, 170, 325
Crowther, P. A., Hillier, D. J., & Smith, L. J. 1995a, A&A, 293, 403
Crowther, P. A., Smith, L. J., Hillier, D. J., & Schmutz, W. 1995b, A&A, 293, 427
Drissen, L., Moffat, A. F. J., Bastien, P., Lamontagne, R., & Tapia, S. 1986, ApJ, 306, 215
Grandchamps, A., & Moffat, A. F. J. 1991, in IAU Symp. 143, Wolf-Rayet Stars and Interrelations with Other Massive Stars in Galaxies, ed. K. A. van der Hucht & B. Hidayat (Dordrecht: Kluwer), 258
Herrero, A. 1993, Space Sci. Rev., 66, 137
Herrero, A., Kudritzki, R. P., Vilchez, J. M., Kunze, D., Butler, K., & Haser, S. 1992, A&A, 261, 209
Howarth, I. D., & Prinja, R. K. 1989, ApJS, 69, 527
Kartasheva, T. A., & Snezhko, L. I. 1985, Soviet Astron., 29(4), 440
Kartasheva, T. A., & Svechnikov, M. A. 1990, Bull. Spec. Astr. Obs.–North Caucasus, 28, 1
Leung, K.-C., Moffat, A. F. J., & Seggewiss, W. 1983, ApJ, 265, 961
Lewis, D., Moffat, A. F. J., Matthews, J. M., Robert, C., & Marchenko, S. V. 1993, ApJ, 405, 312
Lipunova, N. A., & Cherepashchuk, A. M. 1982, Soviet Astron., 26, 569
Marchenko, S. V., Moffat, A. F. J., & Koenigsberger, G. 1994, ApJ, 422, 810
Mathys, G. 1988, A&AS, 76, 427
———. 1989, A&AS, 81, 237
Niemela, V. S. 1980, in IAU Symp. 88, Close Binary Stars Observations and Interpretation, ed. M. J. Plavec, D. M. Popper, & R. K. Ulrich (Dordrecht: Reidel), 177
Penny, L. R., Bagnuolo, W. G., & Gies, D. R. 1993, Space Sci. Rev., 66, 323
Piirola, V., & Linnaluoto, S. 1988, in Polarized Radiation of Circumstellar Origin, ed. G. V. Coyne, et al. (Vatican: Vatican Obs.), 655
Pollock, A. M. T., Haberl, F., & Corcoran, M. F. 1994, in IAU Symp. 163, Wolf-Rayet Stars: Binaries, Colliding Winds, Evolution, ed. K. A. van der Hucht & P. M. Williams (Dordrecht: Kluwer), 512
Schmidt-Kaler, Th. 1982, in Landolt-Börnstein, New Series, Group 6, Vol. 2b, ed. K. Schaiffers & H. H. Voigt (Berlin: Springer), 1
Shore, S. N., & Corcoran, M. F. 1992, in IAU Symp. 151, Evolutionary Processes in Close Binary Systems, ed. Y. Kondo, R. F. Sistero, & R. S. Polidan (Dordrecht: Kluwer), 359
Smith, L. F. 1968, MNRAS, 138, 109
Smith, L. F., Shara, M. M., & Moffat, A. F. J. 1995, MNRAS, submitted
Stevens, I. R., Blondin, J. M., & Pollock, A. M. T. 1992, ApJ, 386, 265
Stickland, D. J., Bromage, G. E., Budding, E., Burton, W. M., Howarth, I. D., Jameson, R., Sherrington, M. R., & Willis, A. J. 1984, A&A, 134, 45
St-Louis, N. 1990, Ph.D. thesis, Univ. College, London
Underhill, A. B., Gilroy, K. K., & Hill, G. M. 1990, ApJ, 351, 651

van der Hucht, K. A., Hidayat, B., Admiranto, A. G., Supelli, K. P., & Doom, C. 1988, A&A, 199, 217
Walborn, N. R. 1974, ApJ, 189, 269
Walborn, N. R., & Fitzpatrick, E. L. 1990, PASP, 102, 379
Walborn, N. R., Nichols-Bohlin, J., & Panek, R. J. 1985, NASA Ref. Publ. No. 1155
Walder, R. 1994, in IAU Symp. 163, Wolf-Rayet Stars: Binaries, Colliding Winds, Evolution, ed. K. A. van der Hucht & P. M. Williams (Dordrecht: Kluwer), 420
Walker, E. N., Lloyd, C., Pike, C. D., Stickland, D. J., & Zuiderwijk, E. J. 1983, A&A, 128, 394